ADAPTIVE-GRID METHODS FOR PHASE FIELD MODELS OF MICROSTRUCTURE DEVELOPMENT

Nikolas Provatas[†,*], Nigel Goldenfeld[*] and Jonathan A. Dantzig[†]
[†]Department of Mechanical and Industrial Engineering
[*]Department of Physics
University of Illinois at Urbana-Champaign

Dendrites are the primary component of solidification microstructures in metals. Their properties have been a topic of intense study in the past 10-15 years. Experiments [1,2] by Glicksman and coworkers on succinonitrile (SCN) and other transparent analogues of metals have provided tests of theories of dendritic growth, and have stimulated considerable theoretical progress [3–5]. The experiments have clearly demonstrated that naturally growing dendrites possess a unique steady state tip, characterized by its velocity, radius of curvature and shape, which leads the to a time-dependent sidebranched dendrite as it propagates.

Insight into the steady state dendrite problem was first obtained from local models [6–9] describing the evolution of the interface, and incorporating the features of the bulk phases into the governing equation of motion for the interface. These models showed that a nonzero dendrite velocity is obtained only if a source of anisotropy – for example, anisotropic interfacial energy – is present in the description of dendritic evolution. It was then shown that the spectrum of allowed steady state velocities is discrete, not continuous, and the role of anisotropy was understood theoretically, both in the local models and the full moving boundary problem [5,10,11]. Moreover, only the fastest of a spectrum of steady state velocities is stable, thus forming the operating state of the dendrite. It is widely believed that sidebranching is generated by thermal or other statistical fluctuations on a microscopic scale, which are amplified by advective diffusion. This body of theoretical work is generally known as solvability theory.

Brute force solution of the time-dependent Stefan problem requires front tracking and lattice deformation to contain the interface at predefined locations on the grid [12]. The *phase-field* model avoids this problem by introducing an auxiliary continuous order parameter $\phi(\mathbf{r})$ that couples to the evolution of the thermal field. The phase field interpolates between the solid and liquid phases, attaining two different constant values in either phase, with a rapid transition region in the vicinity of the solidification front. The level set of $\phi(\mathbf{r}) = 0$ is identified with the solidification front, and the dynamics of ϕ are designed to follow the evolving solidification front [13–23]. The phase-field parameters can be derived from parameters of the Stefan problem [14,24], however this mapping is not very sensitive to the precise form of the phase-field model [25].

While the phase-field model finesses the problem of front tracking, it is still prohibitively expensive for large systems, because the grid spacing must be small enough everywhere that the phase-field model converges to the the sharp interface limit [14,24]. Caginalp and Chen [26] showed rigorously that the phase field model converges to the sharp interface limit when the interface width (and hence the grid spacing) is *much smaller* than the capillary length. This result is necessary for acceptance of the phase field model, but is not sufficient for computational tractability in the experimentally relevant regime.

However, more recently Karma and Rappel [24] presented a different asymptotic analysis in powers of the ratio of the interface width to the diffusion length. Their procedure allows selection of parameters such that the phase field model corresponds to the sharp interface limit when the interface width (and hence the grid spacing) is *of order* the capillary length - a much more tractable

regime. Furthermore, their improved analysis allows the kinetic coefficient to be tuned to zero, which corresponds to the experimentally realized situation at low undercooling in succinonitrile [2]. Karma and Rappel's numerical results are in excellent agreement with solvability theory at dimensionless undercoolings as low as 0.30, but fail to access the range of experimentally-realizable undercoolings near 0.1. What is needed is an effective adaptive technique [27] which dynamically coarsens the grid spacing away from the front.

In this work we show how the phase field model can be solved in a computationally efficient manner that opens a new large-scale simulational window on solidification physics. Our method uses a finite element, adaptive-grid formulation, and exploits the fact that the phase and temperature fields vary significantly only near the interface. We illustrate how our method allows efficient simulation of phase-field models in very large systems, and verify the predictions of solvability theory at intermediate undercooling. We then present new results at low undercoolings that suggest that solvability theory may not give the correct tip speed in that regime.

We model solidification using the phase-field model used by Karma and Rappel [24]. We rescale temperature T by $U = c_P(T - T_M)/L$, where c_P is the specific heat at constant pressure, L is the latent heat of fusion and T_M is the melting temperature. The order parameter is defined by ϕ, with $\phi = 1$ in the solid, and $\phi = -1$ in the liquid. The interface is defined by $\phi = 0$. We rescale time by τ_o, a time characterizing atomic movement in the interface, and length by W_o, a length characterizing the liquid–solid interface. The model is given by

$$\frac{\partial U}{dt} = D\nabla^2 U + \frac{1}{2}\frac{\partial \phi}{\partial t} \tag{1}$$

$$A^2(\vec{n})\ \frac{\partial \phi}{dt} = \nabla \cdot (A^2(\vec{n})\nabla\phi) + (\phi - \lambda U(1 - \phi^2))(1 - \phi^2)$$

$$+ \quad \frac{\partial}{\partial x}\left(|\nabla\phi|^2 A(\vec{n})\frac{\partial A(\vec{n})}{\partial \phi_{,x}}\right) + \frac{\partial}{\partial y}\left(|\nabla\phi|^2 A(\vec{n})\frac{\partial A(\vec{n})}{\partial \phi_{,y}}\right),$$

where $D = \alpha\tau_o/W_o^2$ and α is the thermal diffusivity, and where λ controls the coupling of U and ϕ. Anisotropy has been introduced in Eqs. (1) by defining the width of the interface to be $W(\vec{n}) = W_o A(\vec{n})$ and the characteristic time by $\tau(\vec{n}) = \tau_o A^2(\vec{n})$ [24], with $A(\vec{n}) \in [0, 1]$, and $A(\vec{n}) = (1 - 3\epsilon)\left[1 + \frac{4\epsilon}{1-3\epsilon}\frac{(\phi_{,x})^4+(\phi_{,y})^4}{|\nabla\phi|^4}\right]$. The vector $\vec{n} = (\phi_{,x}\hat{x} + \phi_{,y}\hat{y})/(\phi_{,x}^2 + \phi_{,y}^2)^{1/2}$ is the normal to the contours of ϕ, and $\phi_{,x}$ and $\phi_{,y}$ represent partial derivatives with respect to x and y. The constant ϵ parameterizes the deviation of $W(\vec{n})$ from W_o. We expect the results to be similar for other definitions of anisotropy [14].

We use the asymptotic relationships given in [24] to select the parameters in Eqs. (1) such that it operates in the sharp interface limit, defined by U at the interface satisfying $U_{\text{int}} = -d(\vec{n})\kappa - \beta(\vec{n})V_n$. The variable $d(\vec{n})$ is the capillary length, κ is the local curvature, $\beta(\vec{n})$ is the interface attachment kinetic coefficient and V_n the normal speed of the interface, all in dimensionless form. In terms of $A(\vec{n})$, $d(\vec{n}) = d_o\left[A(\vec{n}) + \partial_\theta^2 A(\vec{n})\right]$, where $d_o = 0.8839/\lambda$ and θ is the angle between $\vec{n}$ and the x-axis. In this formulation, the constants W_o, τ_o and λ may be chosen so as to simulate arbitrary values of β. In particular, $\lambda = 1.5957D$ makes $\beta = 0$ [24], a limit which is appropriate for SCN.

We compute four-fold symmetric dendrites in a quarter-infinite space, initiated by a small quarter disk of radius R_o centered at the origin. The order parameter is initially set to its equilibrium value $\phi_o(\vec{x}) = -\tanh((|\vec{x}| - R_o)/\sqrt{2})$ along the interface. The initial temperature decays exponentially from $U = 0$ at the interface to $-\Delta$ as $\vec{x} \to \infty$.

We simulate Eqs. (1) on an adaptive grid of linear isoparametric quadrilateral and triangular finite elements, formulated using Galerkin's method. Following Ref. [28], elements are arranged on a

two dimensional quadtree data structure, which makes our code scalable when implemented using dynamic memory allocation. The largest system sizes we have considered thus far correspond to 2D uniform lattices having $2^{17} \times 2^{17}$ grid points. The grid is locally refined to have a higher density of elements in the vicinity of the interface, identified by large fluxes in a composite field based on both ϕ and U. Typically, the grid is adapted about every 100 time steps, which permits ϕ and U to remain within the refined range between regriddings. We allow a difference of at most one level of refinement between neighboring quadrilateral elements. In such a case the quadrilateral element of lower level of refinement has an extra side node. The extra nodes are resolved with triangular elements.

On an adaptive grid, the concept of a grid spacing is replaced by that of a minimum grid spacing Δx_{min}, representing the finest level of spatial resolution. We found that for solutions to converge properly, the grid must be *layered* such that the highest density of elements appears around the ϕ interface, while the U-field, whose width is of order D/V_n can be encompassed by a mesh of larger grid spacing. Convergence of our solutions is relatively insensitive to Δx_{min}. For a test case of dendrites grown at $\Delta = 0.55$, $D = 2$, $\epsilon = 0.05$, and integration time step $dt = 0.016$, our solutions for the steady state velocity converge to that given by solvability theory to within a few percent for $0.3 \leq \Delta x_{min} \leq 1.6$.

Fig. 1 shows a dendrite 10^5 time steps into its evolution computed using our adaptive grid method, using the parameters just mentioned above. The system size is 800×800, with $\Delta x_{min} = 0.78$, and about half of the computational domain is shown. Sidebranching is evident, and arises due to numerical noise. This calculation took approximately 10 cpu-hours on a Sun UltraSPARC 2200 workstation.

We examined the cpu-scalability of our algorithm with system size by growing dendrites in systems of various linear dimension L_B and measuring the cpu time R_t^a for the dendrite branches to traverse the entire system. We once again use the same parameters as above, except $\Delta x_{min} = 0.4$. The relationship between R_t^a and L_B is shown in Fig. 2, where we see that $R_t^a \sim L_B^2$. The number of calculations performed, per time step, is proportional to the number of elements in our grid, which is set by the arclength of the interface being simulated multiplied by the diffusion length D/V_n. For a parabolic shape the arclength $\sim L_B$. Thus, since the dendrite tip moves at a constant velocity V_n, then $R_t^a = [R_o^a D V_n^2 / \Delta x_m^2] L_B^2$, where R_o^a is a constant that depends on the implementation. The cpu time R_t^u needed to compute the same case on a uniform grid scales as $R_t^u = [R_o^u / (V_n \Delta x_m^2)] L_B^3$. For large system sizes, $R_t^a / R_t^U \sim L_B$.

We tested the effective anisotropy of our dynamically adapting lattice in two ways. Following the method outlined by Karma [24], we find an equilibrium shape for the interface when the background field is adjusted dynamically so as to maintain the velocity of the interface at zero. The effective anisotropy is inferred by fitting an equation to the computed interface. We found ϵ_{eff} to be within 5% of the intended value for input $\epsilon = 0.02 - 0.04$. We also tested for grid anisotropy by rotating the grid by 45 degrees, which should represent the lowest accuracy for square elements. In this case, the steady state tip-velocity was within 1% of its value in the original orientation.

We further verified our algorithm by comparing measured tip-velocities and shapes for dendrites grown using the same undercoolings, parameter sets and systems sizes reported in [24]. We found very good agreement for $\Delta = 0.65, 0.55, 0.45, 0.30$. We next investigated the effect of system size. Fig. 3 shows the time evolution of tip-velocity for several undercoolings and system dimensions. The two cases for $\Delta = 0.65$ are typical of results at intermediate Δ, showing a relatively rapid leveling to an asymptotic speed within a few percent of that predicted by solvability theory.

At lower Δ, however, we found that the tip-velocity deviates from that predicted by solvability

theory. Fig. 3 also shows the evolution of the tip-velocity for $\Delta = 0.25$ in two different sized boxes. Whereas the computed tip-velocity falls a few percent below the solvability value in the 6400×400 box, it exceeds by 8% the solvability value in the 6400×3200 box. This effect is even larger at $\Delta = 0.1$, also shown in Fig. 3, where the tip speed is about 3 times larger than that predicted by solvability theory.

The explanation for this behavior is that at low Δ, the thermal fields of the two dendrite branches overlap, violating the assumptions of solvability theory, which models an isolated single dendrite. At large undercooling, each dendrite arm quickly outruns the other's thermal boundary layer, and solvability theory should apply. (See Fig. 1, $\Delta = 0.65$.) The conditions of solvability theory can also be approximated at lower undercooling if simulations are performed in a domain which is small in one direction. For the simulation performed with $\Delta = 0.25$ in the small box (6400×400), the branch in the y-direction is extinguished by its interaction with the wall and agreement with solvability theory is obtained. However, when both branches are present, as in the simulation with $\Delta = 0.25$ in the larger box (6400×3200), their interaction leads to an increased tip-velocity because the dendrites are embedded in a circular rather than parabolic diffusion field. This is clearly seen in Fig. 4, where the dendrite shape and its associated field are shown for $\Delta = 0.10$ ($D = 13$, $d_0 = 0.043$, $\epsilon = 0.05$, $\Delta x = 0.78$, $dt = 0.08$). The dendrite arms never became free of each other in this simulation, causing the observed deviation from solvability theory shown in Fig. 3. This latter simulation was performed in a 102400×51200 domain, chosen to contain about $10D/V_n$. We note that the ratio of the largest to smallest element size in this simulation is 2^{17}. A fixed mesh having the same resolution would contain 9×10^9 grid points, clearly beyond current computing capability.

We can estimate the time $t^\star$ when the growth of the dendrite tip crosses over from the transient regime where the branches interact to that where they become independent by equating the length of the full diffusion field, $3(Dt^\star)^{1/2}$, to the length of a dendrite arm, $V_n t^\star$. This gives the crossover time as $t^\star = 9D/V_n^2$. The values for $t^\star$ corresponding to the cases $\Delta = 0.65$, 0.25 and 0.10 in Fig. 3 are 2.5×10^3, 1.6×10^4 and 5.9×10^7, respectively. Inspection of Fig. 3 confirms this scaling.

These results have important implications when comparing theory to experimental observations at low undercooling. We find that in this regime, the appropriate theory to use is one which explicitly takes into account the long range effects of other branches [29]. In particular, study of real dendrites with sidebranches, growing at low undercooling, will require such treatment. An investigation of this effect, as well as results in 3D, applications to directional solidification and other solidification processes, and a more detailed description of our algorithm will appear in future publications.

References

[1] S.-C. Huang and M.E. Glicksman, Acta. Metall., 29, 701 (1981)]

[2] M. E. Glicksman, Materials Science and Engineering, 65 (1984).

[3] J.S. Langer, Rev. Mod. Phys. 52, 1 (1980);

[4] J.S. Langer, "Lectures in the Theory of Pattern Formation", in *Chance and Matter*, Les Houches Session XLVI, edited by J. Souletie, J. Vannenimus and R. Stora (North Holland, Amsterdam, 1987), p. 629.

[5] D.A. Kessler, J. Koplik and H. Levine, Adv. Phys. **37**, 255 (1988).

[6] R. Brower, D. Kessler, J. Koplik, and H. Levine, Phys. Rev. Lett., **51**, 1111, (1983).

[7] E. Ben-Jacob, N. Goldenfeld, J.S. Langer and G. Schön, Phys. Rev. Lett., **51**, 1930 (1983).

[8] E. Ben-Jacob, N. Goldenfeld, B.G. Kotliar, and J.S. Langer, Phys. Rev. Lett., **53**, 2110 (1984).

[9] D. Kessler, J. Koplik, and H. Levine, Phys. Rev. A, **30**, 3161 (1984).

[10] E. Brener, and V. I. Melnikov, Adv. Phys. **40**, 53 (1991).

[11] Y. Pomeau and M. Ben Amar, *Dendritic growth and related topics*, in *Solids far from equilibrium*, ed. C. Godrèche, (Cambridge, 1991) 365.

[12] R. Almgren, J. Comp. Phys. **106**, 337 (1993).

[13] J. S. Langer, in *Directions in Condensed Matter* (World Scientific, Singapore, 1986), 164.

[14] G. Caginalp, Arch. Rat. Mech. Anal. **92**, 205 (1986); G. Caginalp, Anal. of Phys. **172**, 136 (1986); G. Caginalp, and E. Socolovsky, SIAM J. Sci. Comp. **15**, 106 (1991).

[15] J. B. Collins and H. Levine, Phys. Rev. B, **31**, 6119 (1985).

[16] J. A. Warren and W. J. Boettinger, Acta Metall. Mater. A **43**, 689 (1995)

[17] A. A. Wheeler, W.J. Boettinger, and G. B. McFadden Phys. Rev. A **45**, 7424 (1992) (1996).

[18] A. Karma, Phys. Rev. E **49**, 2245 (1994).

[19] K. R. Elder, F. Drolet, J. M. Kosterlitz, and M. Grant, Phys. Rev. Lett. **72**, 677 (1994).

[20] A. A. Wheeler, G. B. McFadden, and W.J. Boettinger, Proc. Royal Soc. London A **452**,

[21] R. Kobayashi, Physica D **63**, 410 (1993).

[22] N. Provatas, E. Elder, M. Grant, Phys. Rev. B, **53**, 6263 (1996).

[23] S-L. Wang and R. F. Sekerka, Phys. Rev. E **53**, 3760 (1996).

[24] A. Karma, and W.-J. Rappel, Phys. Rev. E **53**, 3017 (1995); A. Karma, and Wouter-Jan Rappel, Preprint (1997).

[25] M. Fabbri and V. R. Voller, J. Comp. Phys. **130**, 256 (1997).

[26] G. Caginalp and X. Chen, *On The Evolution Of Phase Boundaries*, edited by M.E. Gurtin an d G.B. McFadden (Springer-Verlag, New York, 1992), p.1.

[27] R. J. Braun, and B. T. Murray, J. Cryst. Growth **174**, 41 (1997).

[28] N. Palle, and J. A. Dantzig, Met. Trans. A, **27A**, 707 (1996).

[29] R. Almgren, W. S. Dai and V. Hakim, Phys. Rev. Lett., **71**, 3461 (1993).
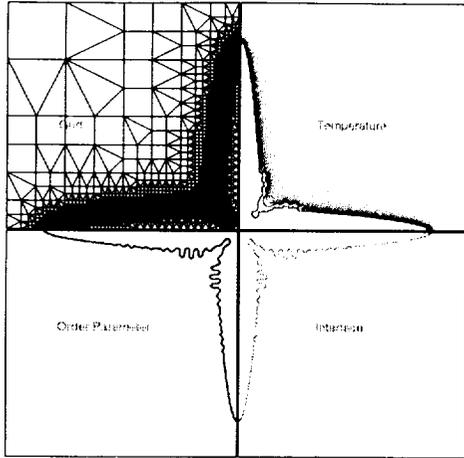
Figure 1: A dendrite grown using the adaptive-grid method for $\Delta = 0.55$, $D = 2$, $\epsilon = 0.05$. Clockwise, beginning at the upper right the figures show contours of the U-field, the contour $\phi = 0$, contours of the ϕ-field and the current mesh.
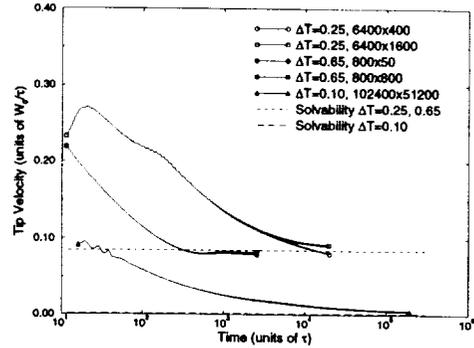
Figure 3: The time evolution of the tip-velocity for undercooling $\Delta = 0.65, 0.25$ and 0.10.
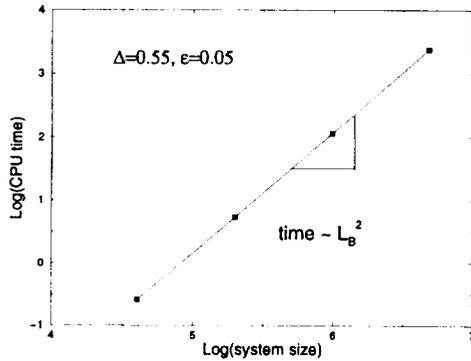
Figure 2: CPU time vs. the system size, illustrating the computing time for a dendrite to move through the system of linear dimension L_B using our adaptive mesh method.
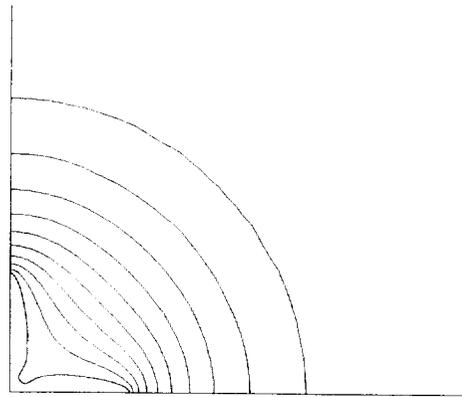
Figure 4: Dendrite silhouette and isotherms from -0.01 to -0.9 for undercooling $\Delta T = 0.1$. Full domain dimensions are $102,400 \times 51,200$. The dendrite tip is approximately $1,300$ units from the origin, while the temperature field spreads to about $5,000$ units.